

Supplementary Information File

Inducing molecular orientation in solution processed thin films of fluorene-bithiophene-based copolymer: the effect of thermal annealing, insulating matrix confinement and solvent additive

Cassia Ferreira Coutinho Pereira¹, Bruno G. A. L. Borges¹, Karlison R. A. Sousa^{2,3}, Soheila Holakoei¹, Lucimara S. Roman², C. Moyses Araujo^{5,6}, Marco Cremona⁴, Marlus Koehler², Cleber Marchiori^{5*} and Maria Luiza M. Rocco^{1*}

¹Institute of Chemistry, Federal University of Rio de Janeiro (UFRJ), 21941-909, Rio de Janeiro-RJ, Brazil.

²Department of Physics, Federal University of Paraná (UFPR), Centro Politécnico, CP 19081, 81531-900, Curitiba-PR, Brazil.

³Fundação de Amparo à Pesquisa do Estado do Amazonas – FAPEAM, 69058-030, Manaus - AM, Brasil

⁴Departamento de Física, PUC-Rio, 22453-900, Rio de Janeiro-RJ, Brazil.

⁵Department of Engineering and Physics, Karlstad University, 65188 Karlstad, Sweden.

⁶Materials Theory Division, Department of Physics and Astronomy, Uppsala University, 75120 Uppsala, Sweden.

This Supporting Information is composed of the following sections:

1. Supporting Figures (Figure S1 to Figure S11).
2. Supporting Tables (Table S1 to S5).

Figure Captions

Figure S1 – XPS survey spectra of F8T2 pristine, annealed and processed with DIO polymeric films.

Figure S2 – C1s XPS core-level spectra of, respectively, F8T2, F8T2 annealed film and F8T2 film processed with DIO.

Figure S3 – Sulfur K-edge NEXAFS spectrum of F8T2 (black) and its corresponding second derivative graph (blue).

Figure S4 – Angular dependence of Sulfur K-edge TEY NEXAFS [(a) and (c)] and difference [(b) and (d)] spectra for, respectively, the F8T2 annealed and DIO processed F8T2 polymeric films.

Figure S5 – Sulfur $KL_{2,3}L_{2,3}$ Auger decay spectra obtained for photon energies labeled as A-D in the NEXAFS spectrum of F8T2 for: a) F8T2 film as cast; b) thermally annealed F8T2 film b) F8T2 film additive processed.

Figure S6 – Snapshots of oligomers throughout the simulation of CB evaporation. The system consists of 100 oligomers of F8T2 containing 16 repeating units, and solvent CB and DIO (both omitted for better visualization of the solute).

Figure S7 – Population of F8T2 oligomers as a function of the dihedral angle ϕ between the thiophenes' rings of the BT moiety. The yellow curve refers to the distribution in the blue curve represents the final distribution after the solvent evaporation.

Figure S8 – a) Radial distribution of pairs between sulfur (F8T2) and iodine (DIO) atoms for some moments of the solvent evaporation simulation. b) Mean distances between sulfurs and iodines during MD. c) Radial Distribution Function $g(r_{ij})$ between the sulfur atoms in the BT moiety and the alkyl chains attached to the FL group.

Figure S9 – Some examples of configurations of oligomers' dimers (or single oligomer's chains) taken from the film after the MD evaporation with DIO. Those configurations illustrate some situations where there is a proximity between atoms of the lateral alkyl chains with the BT ring of the oligomer.

Figure S10 – Simplified two-dimensional model representing the electrostatic environment filled by the S atom (represented by the points S and S') in the vicinities of an alkyl lateral chain of the F8T2 oligomer. The coordinates r_{FL-S} (r'_{FL-S}) and \bar{r}_{FL-S} (\bar{r}'_{FL-S}) are the distances of S (S') to the center of the reference system and the average distance to the point charges in the nearest octyl side chain, respectively. The atomic charges are represented by net point charges with magnitudes given by DFT calculations. The coordinates of the alkyl charges are also in accordance with bond lengths and angles extracted from DFT. The FL point in the origin is associated to the net charge of the central pentagonal ring of the FL group whereas the FL2 represents the net charge on the remaining three carbon atoms of hexagonal ring (considering an average distance of those atoms to origin as given by DFT). Finally, the point Th represents the net charge of the closest thiophene ring belonging to the BT

group. To preserve the symmetry of the system, the points FL2 and Th are also considered in the $x < 0$ interval. See Table S22 for details of charge coordinates and magnitudes.

Figure S11 – Illustration of the basic model based on the Born's theory of ion-solvent interaction to estimate the electric field variation ΔF produced by a $+\Delta q$ charge increase in a central point charge representing the S atom. See text for more details.

Table Captions

Table S1 – Peak assignment and chemical composition for the C1s XPS spectra of the F8T2, F8T2-T, and F8T2-DIO films.

Table S2 – Peak assignment and chemical composition for the S2ps XPS spectra of the F8T2, F8T2-T, and F8T2-DIO films.

Table S3 – Values adapted from the OPLS table for parametrization of the CB, DIO molecules and oligomer of F8T2, in the united atoms (UA) model, available in the GROMACS package directory. The CB and F8T2 partial atomic charges were obtained from geometry optimizations employing DFT/ ω B97XD/6-31G(d,p)^[13] and DFT/LanL2MB/6-31G(d,p) just for DIO, all in ESP formalism.

Table S4 – Average number of groups (n) present in a spherical volume with center in a specific moiety of the chain and $r = 8 \text{ \AA}$ for the final films *formed* with and without DIO.

Table S5 – Positions and charges of the point charges used scheme of Figure 14. The charges are taken from DFT calculations of F8T2 oligomers assuming the Millikan approximation, and wb97xd (6-31g**) level of theory.

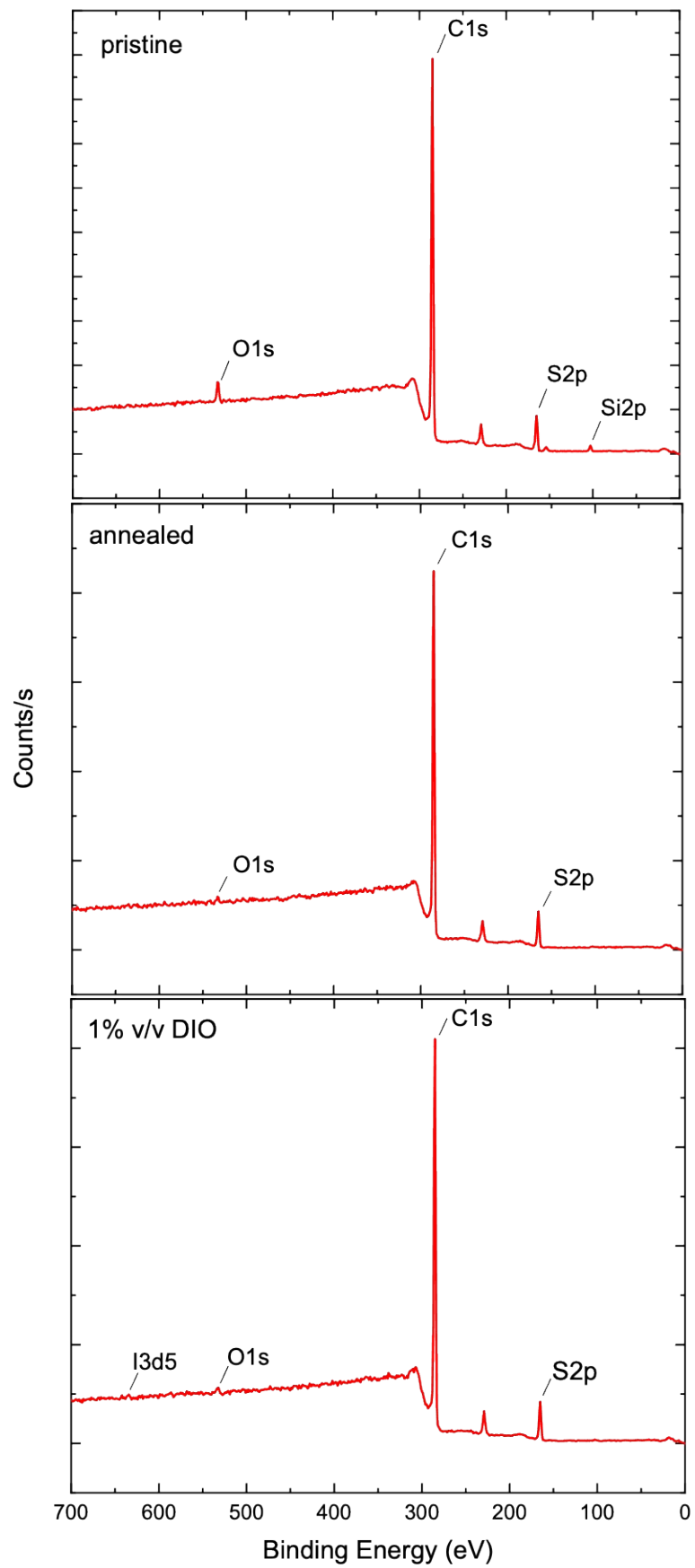


Figure S1 - XPS survey spectra of F8T2 pristine, annealed and processed with DIO polymeric films.

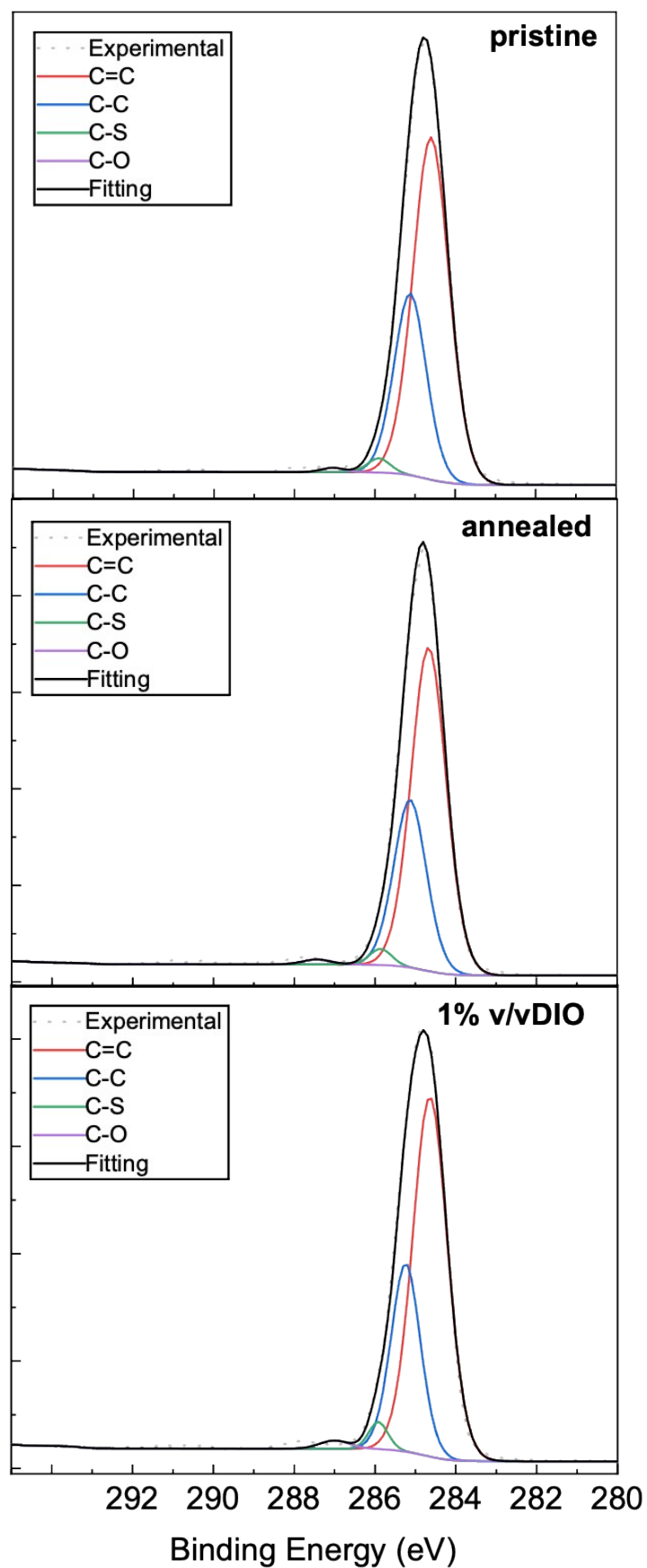


Figure S2 - C₁s XPS core-level spectra of, respectively, F8T2, F8T2 annealed film and F8T2 film processed with DIO.

Table S1 - Peak assignment and chemical composition for the C1s XPS spectra of the F8T2, F8T2-T, and F8T2-DIO films.

| C1s | Binding Energy (eV) | FWHM (eV) | Atomic % |
|-----------------|----------------------------|------------------|-----------------|
| F8T2 | | | |
| C=C | 284.6 | 1.06 | 65.00 |
| C-C | 285.1 | 1.06 | 30.46 |
| C-S | 285.9 | 1.35 | 3.46 |
| C-O | 287.1 | 1.35 | 1.08 |
| F8T2-T | | | |
| C=C | 284.7 | 1.02 | 65.41 |
| C-C | 285.1 | 0.95 | 31.68 |
| C-S | 285.9 | 0.64 | 2.05 |
| C-O | 287.4 | 0.83 | 0.85 |
| F8T2-DIO | | | |
| C=C | 284.6 | 1.01 | 66.43 |
| C-C | 285.2 | 0.86 | 29.44 |
| C-S | 285.9 | 0.56 | 2.80 |
| C-O | 287.0 | 0.87 | 1.32 |

Table S2 - Peak assignment and chemical composition for the S2ps XPS spectra of the F8T2, F8T2-T, and F8T2-DIO films.

| S2p | Photon Energy (eV) | FWHM (eV) | Atomic % |
|---------------------------------------|---------------------------|------------------|-----------------|
| F8T2 | | | |
| S2p _{3/2} (S-C) | 163.8 | 0.81 | 15.26 |
| S2p _{1/2} (S-C) | 164.9 | 0.81 | 15.26 |
| S2p _{3/2} (S-C) ⁺ | 164.5 | 0.89 | 33.62 |
| S2p _{1/2} (S-C) ⁺ | 165.7 | 0.89 | 33.63 |
| S2p _{3/2} (SO ₂) | 167.2 | 1.66 | 1.12 |
| S2p _{1/2} (SO ₂) | 168.3 | 1.66 | 1.12 |
| F8T2-T | | | |
| S2p _{3/2} (S-C) ⁺ | 164.4 | 0.93 | 48.83 |
| S2p _{1/2} (S-C) ⁺ | 165.6 | 0.93 | 48.85 |
| S2p _{3/2} (SO ₂) | 167.4 | 0.98 | 1.16 |
| S2p _{1/2} (SO ₂) | 168.5 | 0.98 | 1.16 |
| F8T2-DIO | | | |
| S2p _{3/2} (S-C) ⁺ | 164.4 | 1.03 | 49.10 |
| S2p _{1/2} (S-C) ⁺ | 165.6 | 1.03 | 49.10 |
| S2p _{3/2} (SO ₂) | 167.4 | 0.86 | 0.91 |
| S2p _{1/2} (SO ₂) | 168.5 | 0.86 | 0.91 |

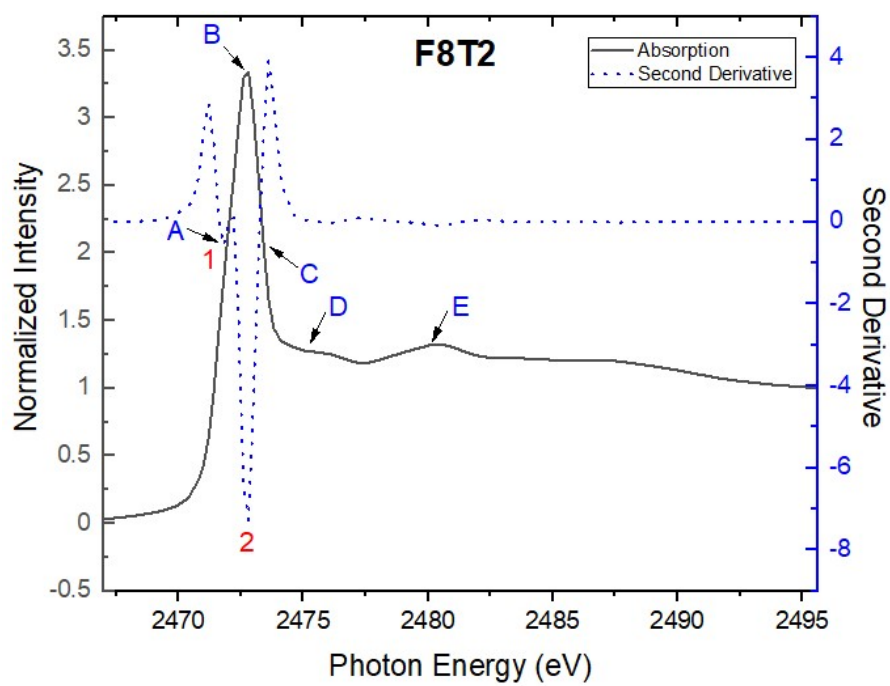


Figure S3 - Sulfur K-edge NEXAFS spectrum of F8T2 (black) and its corresponding second derivative graph (blue).

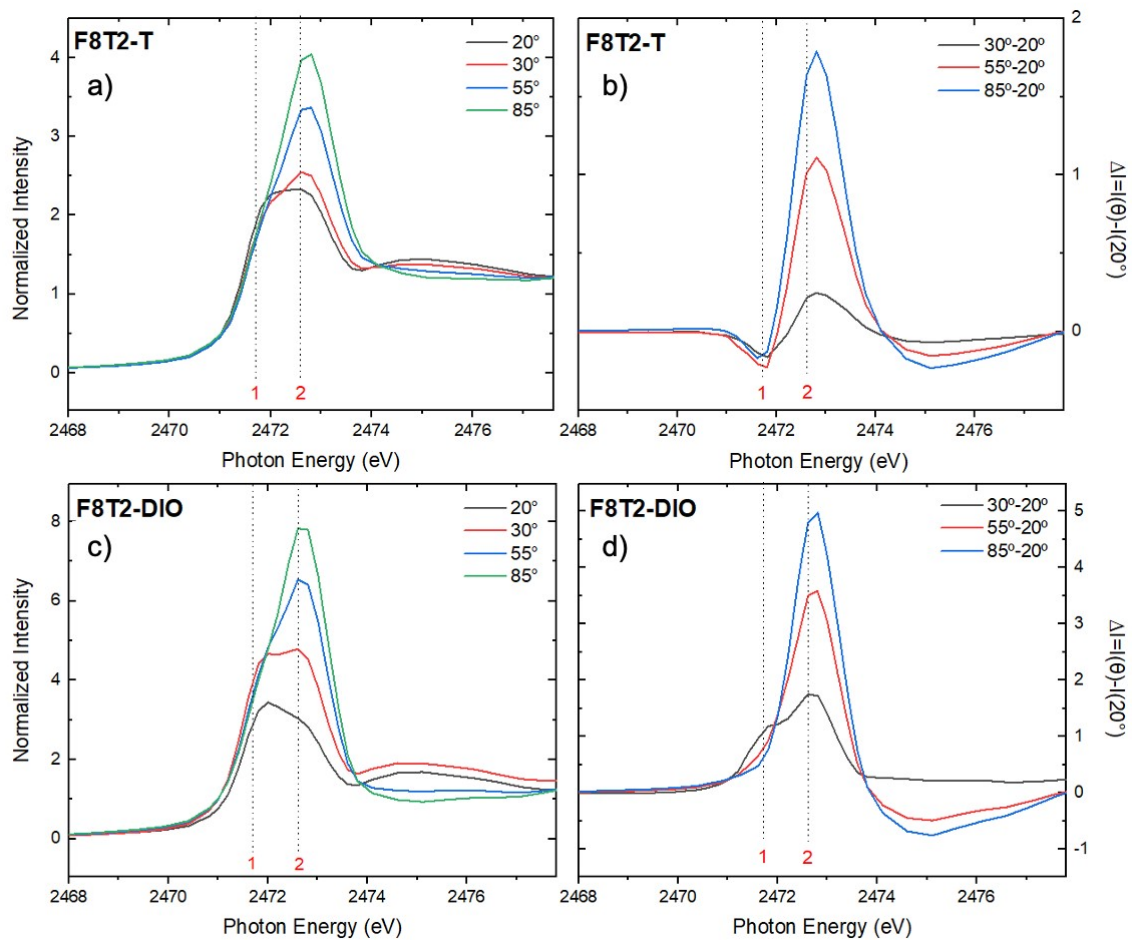


Figure S4 - Angular dependence of Sulfur K-edge TEY NEXAFS [(a) and (c)] and difference [(b) and (d)] spectra for, respectively, the F8T2 annealed and DIO processed F8T2 polymeric films.

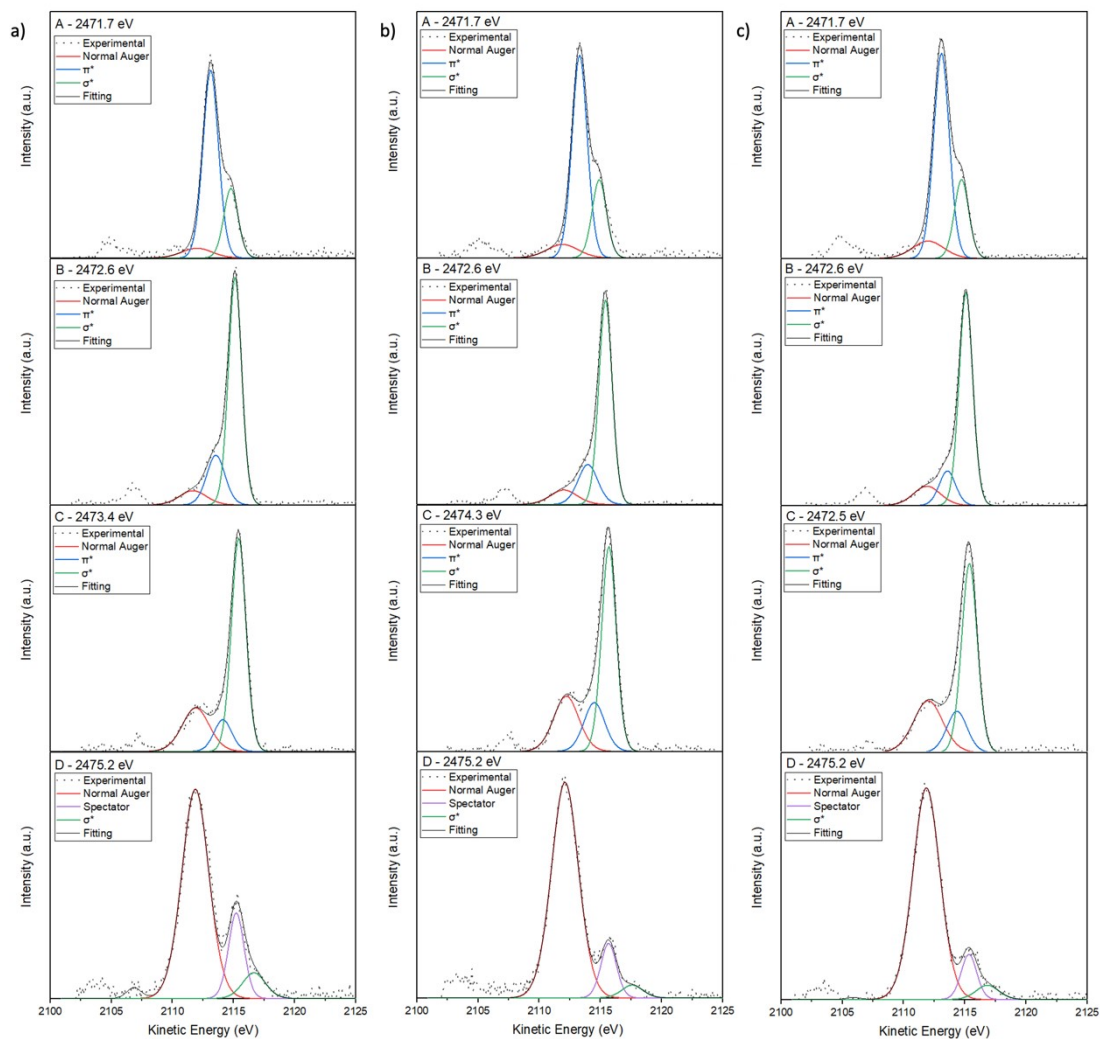


Figure S5 - Sulfur $KL_{2,3}L_{2,3}$ Auger decay spectra obtained for photon energies labeled as A-D in the NEXAFS spectrum of F8T2 for: a) F8T2 film as cast; b) thermally annealed F8T2 film; c) F8T2 film additive processed.

CLASSICAL MOLECULAR DYNAMICS OF THE F8T2/(CB and CB:DIO) SYSTEM

COMPUTATIONAL MODEL

Classical molecular dynamics and the force field

Classical molecular dynamics simulates the temporal dynamics of a system of particles, such as atoms, molecules, or ions, in a defined thermodynamic state, using a mathematical model that describes the classical interactions between particles, known as a force field.

Force field parameters include interaction forces, equilibrium distances, angles of three bonded particles, dihedral angles among four particles, and covalent bonds between pairs of particles. Interaction forces are modeled by energy potentials, such as the Lennard-Jones potential, which describes van der Waals interactions between particles, and the Coulomb potential, which describes electrostatic interactions between charged particles. The equilibrium distances are the values of the distances between particles at which the potential energy is minimum. In summary, the theoretical force field of the present study on a particle i is equivalent to:

$$U_i = \sum_{bonds} \frac{K_l}{2} (l_{ij} - l_0)^2 + \sum_{angles} \frac{K_\theta}{2} (\theta_{ijk} - \theta_0)^2 + \sum_{improper\ dihedrals} \frac{K_\xi}{2} (\xi_{ijkl} - \xi_0)^2 +$$
$$+ \sum_{proper\ dihedrals} \sum_{n=0}^5 C_n \cdot (\cos(\phi_{ijkl}))^n + \sum_{j=1, j>i}^N 4 \cdot \varepsilon_{ij} \left[\left(\frac{\sigma_{ij}}{r_{ij}} \right)^{12} - \left(\frac{\sigma_{ij}}{r_{ij}} \right)^6 \right] \quad (1)$$
$$+ \sum_{j=1, j>i}^N \frac{q_i \cdot q_j}{4\pi\epsilon_0 r_{ij}}.$$

The first three terms on the right side of Eq. (1) are parabolic functions that classically adjust the harmonic motions around an equilibrium point (l_0, θ_0, ξ_0) present in the chemical bond, in the angle and the improper dihedral angle, respectively. The elastic constants $K_{l,\theta,\xi}$ of the harmonic potentials, the interaction energy ε_{ij} and the characteristic diameter σ_{ij} between two particles i and j , were taken from the Optimized

Potential for Liquid Simulations (OPLS) table,^[1,2,3] and the last two parameters are obtained by the standard Lorentz-Berthelot equation,^[4-6] that is, $\epsilon_{ij} = \sqrt{\epsilon_i \cdot \epsilon_j}$ and $\sigma_{ij} = 0.5 \cdot (\sigma_i + \sigma_j)$. The values l_{ij} , θ_{ijk} , ξ_{ijkl} , ϕ_{ijkl} and r_{ij} are calculated during the dynamics.

A torsion along the polymer backbone is implemented by the Ryckaert-Bellemans potential, the fourth term of Equation (1). The function calculates the torsional energy of four atoms at a given angle ϕ_{ijkl} of torsional flexion (proper dihedral angles). The torsional energy profile between the thiophenes of F8T2 was previously obtained through *ab initio* calculations using the Functional Density Theory (DFT) with the functional B3LYP^[7] and the base function 6-31G(d,p).^[8,9] Then an interpolation was performed on this energy profile with the Ryckaert-Bellemans equation to obtain the coefficients C_n .

Finally, the van der Waals and electrostatic interactions are represented by the Lennard-Jones and Coulomb equation, the last two terms of Eq. (1), where the variables q_i, q_j are the partial atomic charges of each particle, in this case, obtained in the ESP^[10,11] formalism.

Force field parametrization

Force field parametrization is a critical process to ensure that simulations produce accurate and reliable results. This is done using experimental or theoretical data to adjust the parameters so that it adequately reproduces the thermodynamic and structural properties of the system under study. Theoretical validation then involves applying this parameterized force field to systems for which there are experimental or theoretical data to compare with simulation results. This helps ensure that the force field can accurately predict the physical properties of the molecules and systems under study.

There are several publicly available force field parametrization tables, including OPLS, which is a force field widely used for simulations of liquids and macromolecules, such as proteins and nucleic acids. He is known for his accuracy in reproducing various properties, including the structure of proteins and the thermodynamics of liquid solutions.

Some values of the main parameters used in the Lennard-Jones equation are shown in **Table S1**. We also use from these tables values of the elastic constants of the chemical bonds and angles.

Theoretical validation of materials

In validating the simulated solvents, the following steps were performed for each system containing 1000 molecules in the UA model. First, an energy minimization of $1 \cdot 10^7$ steps in the steepest descent method was performed to avoid any particle overlaps and the consequent potential energy divergence. Next, a dynamic was performed using the velocity method Verlet^[12] of $1 \cdot 10^7$ steps with an increment of 2.0fs of time in the equations of motion, resulting in 20.0 ns of simulation in the ensemble NPT. Both solvent simulations were performed at an average temperature of 298.15 K and a pressure of 1.0atm. The physical simulation time of 20.0 ns was enough to reach the expected results due to the size of the system and the rapid convergence of its potential energy.

Table S3 – Values adapted from the OPLS table for parametrization of the CB, DIO molecules and oligomer of F8T2, in the united atoms (UA) model, available in the GROMACS package directory. The CB and F8T2 partial atomic charges were obtained from geometry optimizations employing DFT/ ω B97XD/6-31G(d,p)^[13] and DFT/LanL2MB/6-31G(d,p) just for DIO, all in ESP formalism.

| Material | Name | Atom | Mass [μ] | σ_{ij} [nm] | ϵ_{ij} [kJ mol ⁻¹] |
|----------|----------|------|----------------|--------------------|---|
| CB-UA | opls_264 | Cl | 35.453 | 0.340 | 1.255 |
| | opls_145 | C | 12.011 | 0.355 | 0.293 |
| | opls_075 | C | 13.019 | 0.367 | 0.460 |
| DIO-UA | opls_732 | I | 126.904 | 0.367 | 2.426 |
| | opls_110 | C | 14.027 | 0.380 | 0.290 |
| F8T2-UA | opls_633 | S | 32.060 | 0.355 | 1.046 |
| | opls_567 | C | 12.011 | 0.355 | 0.293 |
| | opls_568 | C | 13.019 | 0.367 | 0.293 |
| | opls_009 | C | 14.027 | 0.390 | 0.464 |
| | opls_010 | C | 15.035 | 0.390 | 0.732 |

In validating the simulated solvents, the following steps were performed for each system containing 1000 molecules in the UA model. First, an energy minimization of $1 \cdot 10^7$ steps in the steepest descent method was performed to avoid any particle overlaps and the consequent potential energy divergence. Next, a dynamic was

performed using the velocity method Verlet^[12] of $1 \cdot 10^7$ steps with an increment of 2.0fs of time in the equations of motion, resulting in 20.0 ns of simulation in the ensemble NPT. Both solvent simulations were performed at an average temperature of 298.15K and a pressure of 1.0atm. The physical simulation time of 20.0 ns was enough to reach the expected results due to the size of the system and the rapid convergence of its potential energy.

The analyzed properties are the volumetric density(ρ)and the enthalpy variation of vaporization (ΔH_{vap}) since these two properties are directly influenced by the parameters σ and ϵ of van der Waals interactions. The density of the CB solvent found, for example, was $\rho = 1175.27 \pm 4.81 \text{ kg/m}^3$ with an error of $\simeq + 6.5\%$ compared to the average values in the literature.^[14 - 17] On the other hand, from the equation for the change in enthalpy of vaporization

$$\Delta H_{vap} \simeq [U_{(potential)} + RT]_{gas} - [U_{(potential)} + pV]_{liq}, \quad (2)$$

we have $\Delta H_{vap} = 40.09 \text{ kJ/mol}$ with an error of $\simeq + 1.68\%$.^[14,16,18] The DIO solvent was validated with values of $\rho = 1851.87 \pm 6.77 \text{ kg/m}^3$ (with an error of $\simeq + 2.88\%$ ^[14]) and $\Delta H_{vap} = 54.93 \text{ kJ/mol}$ (with an error of $\simeq - 0.49\%$ ^[14]).

The Evaporation Process

The resulting layer, or thin film, containing only the F8T2 oligomers consists of 100 oligomers containing 16 repeat units each (8.84 kDa each oligomer). Analogously to the experimental method and to the method that we have already used in our previous works,^[19 - 21] the F8T2 oligomers were randomly mixed with the previously equilibrated CB solvent, and in another case, with CB and a small percentage of the volume with DIO. Both simulated systems have $(30.0 \times 30.0 \times 60.0) \text{ nm}^3$ dimensions.

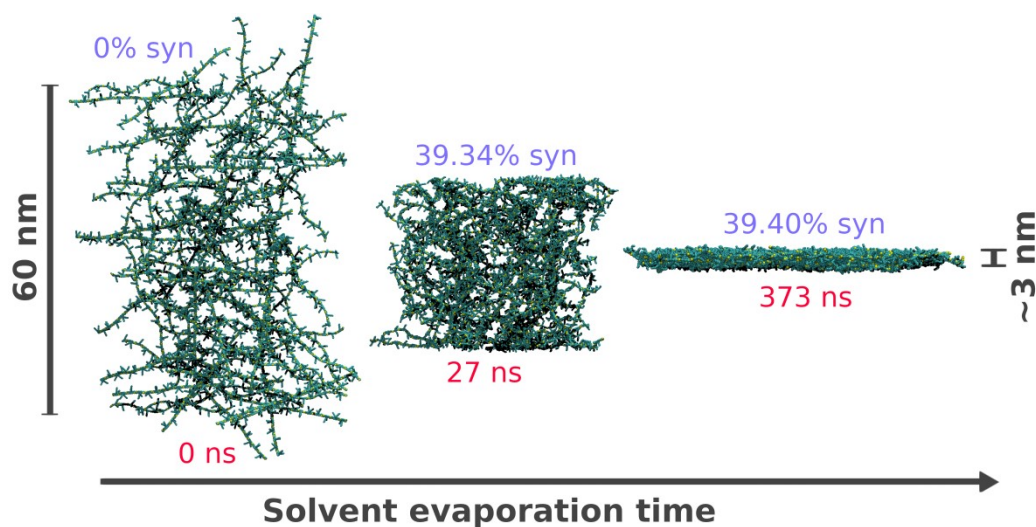


Figure S6 - Snapshots of oligomers throughout the simulation of CB evaporation. The system consists of 100 oligomers of F8T2 containing 16 repeating units, and solvent CB and DIO (both omitted for better visualization of the solute).

The simulation of solvent evaporation was carried out through steps adapted from the protocol provided by Alessandri *et al.*^[22]. In this protocol, many sequential simulations are performed until all the solvent is removed from the system. Between each simulation, 2.0% of CB is removed. The entire MD was performed in the NVT ensemble at a temperature environment and pressure of 1.0 atm. Figure SI5 shows some snapshots of the system during the evaporation process.

Average Number of Groups (n) Interacting with a Moiety

Table S4 – Averagenumberofgroups (n) present in a spherical volume with center in a specificmoietyofthechainand $r = 8 \text{ \AA}$ for the final films formed withandwithout DIO.

| Interaction | n (CB only) | n (with DIO) |
|-------------|---------------|----------------|
| BT-BT | 1.480 | 1.257 |
| FL-BT | 1.477 | 1.373 |
| FL-FL | 1.294 | 1.044 |

Population of Syn and Anti Conformers as a function of the dihedral angle

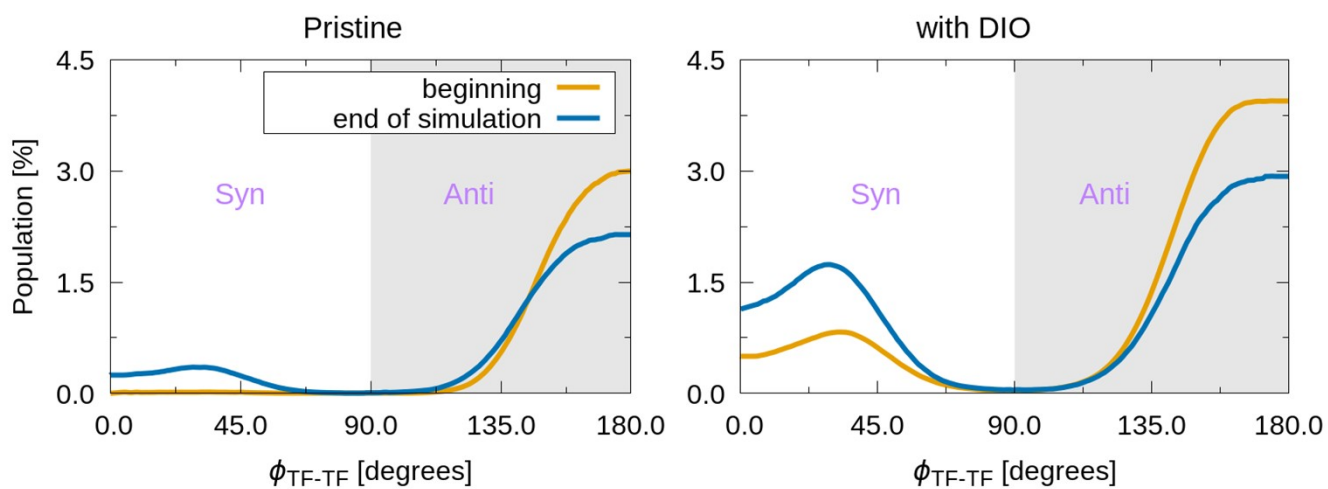


Figure S7– Population of F8T2 oligomers as a function of the dihedral angle ϕ between the thiophenes' rings of the BT moiety. The yellow curve refers to the distribution in the blue curve represents the final distribution after the solvent evaporation.

Radial Distribution Function between the S atoms and the Octyl Chains

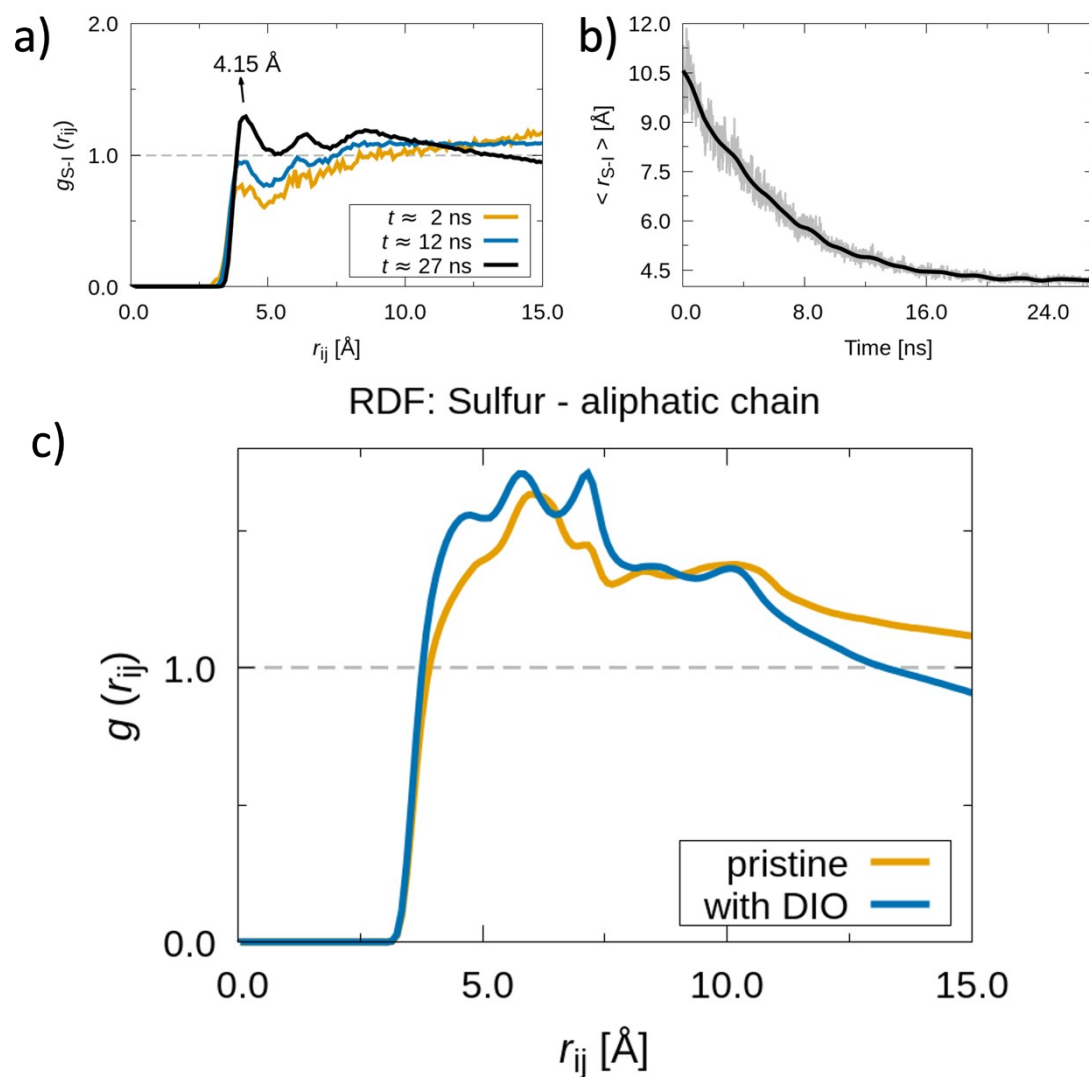


Figure S8 - a) Radial distribution of pairs between sulfur (F8T2) and iodine (DIO) atoms for some moments of the solvent evaporation simulation. b) Mean distances between sulfurs and iodines during MD. c) Radial Distribution Function $g(r_{ij})$ between the sulfur atoms in the BT moiety and the alkyl chains attached to the FL group.

Some Molecular Configurations After the MD Evaporation with DIO

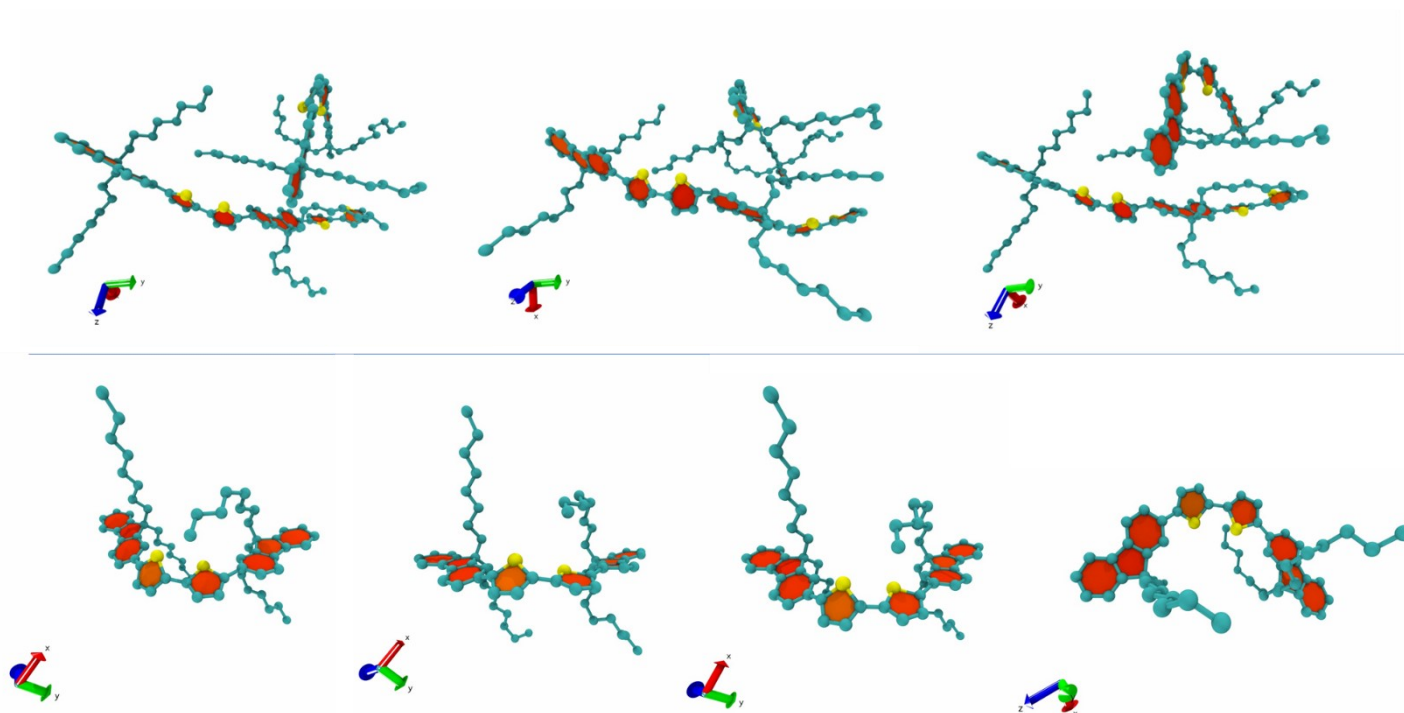


Figure S9 - Some examples of configurations of oligomers' dimers (or single oligomer's chains) taken from the film after the MD evaporation with DIO. Those configurations illustrate some situations where there is proximity between atoms of the lateral alkyl chains with the BT ring of the oligomer.

Basic Modelling to Access Electrostatic Environmental Variations around the BT Group

Effective Nuclear Charge and Born's approach to estimate ΔF

We begin by assuming that the higher binding energy detected in the sulfur atoms after the use of DIO is due to an excess positive charge felt by the core 2p electrons of the S atom. To quantify the magnitude of charge variation necessary to produce a 0.7 eV shift in the XPS spectra, we will apply a crude model of a multielectron atom that is essentially based on the solutions for the hydrogen atom^[24]. In this approach the variations in the BE are related to effective nuclear charge (Z_{eff}) that takes into account the electrostatic shielding effect produced by the negatively charged electrons in the inner shells of the atom. In this model, the modulus of the electron binding energy and its average separation from the nucleus are, respectively:

$$E_n \approx \left(\frac{Z_{eff}}{n} \right)^2 E_0, \quad (1)$$

$$\bar{r} \approx \frac{n^2}{Z_{eff}} a_0, \quad (2)$$

where n is the principal quantum number (for 2p electrons $n = 2$), E_0 is the ground state energy of hydrogen atom ($E_0 = 13.6$ eV), and a_0 the Bohr radius ($a_0 = 0.5$ Å). Using Eq. (1), it is possible to calculate the variation of the effective nucleus charge ($\Delta Z_{eff} = Z'_{eff} - Z_{eff}$, where Z'_{eff} is the effective charge for the higher BE) necessary to produce the difference from 163.8 eV to 164.5 eV (+0.7 eV energy shift) in the XPS peaks. It was found that $\Delta Z_{eff} \approx 0.0148$ which directly gives the amount of excess positive charge $\Delta q = \Delta Z_{eff} e$, where e is the elementary charge. Applying Eq. (2), it is possible to estimate the average displacement of the electronic cloud necessary to induce Δq , or

$$\Delta \bar{r} \approx \frac{\Delta Z_{eff}}{Z'_{eff} Z_{eff}} n^2 a_0. \quad (3)$$

We assume that Δq and $\Delta \bar{r}$ are generated by an extra polarization $\Delta \mu$ of the atom due to a change ΔF in electric field surrounding the thiophene ring. Since $\Delta \mu = \Delta q \bar{r} + (Z_{eff} e) \Delta \bar{r}$, ΔF is

$$\Delta F = \frac{\Delta \mu}{\alpha} \approx \left[\frac{Z'^2_{eff} - Z^2_{eff}}{Z'_{eff} Z_{eff}} \right] \frac{n^2 a_0 e}{\alpha}, \quad (4)$$

where α is the average polarizability of the sulfur atom. Taking the values of Z'_{eff} (Z_{eff}) from the XPS binding energies, and $\alpha = 24 a_0^3$ ^[25], Eq. (4) gives $\Delta F \approx 0.035$ V/Å.

We also tested another argument to access ΔF using the simple model based on Born's approach^[26] to the ion-solvent interaction. This theory estimates the stabilization energy for the ion-solvent system assuming a charged sphere of radius r_i immersed in a continuum dielectric media of relative dielectric constant ϵ_r . The S atom is assumed to be in the center of a spherical vacuum cavity within the dielectric media. Any excess charge in S is compensated by a charge with opposite sign in the dielectric to keep electrostatic neutrality (see Fig S11). In this picture, the energy necessary to stabilize the sphere with charge $Z_{eff} e$ is simply $G = - (Z_{eff} e / 8\pi \epsilon_0 r_i^2) (1 - \epsilon_r^{-1})$, where ϵ_0 is the vacuum permittivity. If the average radius of the "solvation layer" is assumed constant, the additional charge $\Delta Z_{eff} e$ induced in the S atom implies to an extra energy $\Delta G = - (\Delta Z_{eff} e / 8\pi \epsilon_0 r_i^2) (1 - \epsilon_r^{-1})$ to stabilize the ion-dielectric system. The average electric field necessary to perform the extra work to charge the sphere by $\Delta Z_{eff} e$ is assumed $\Delta F = - \Delta G / e r_i$. For $r_i = 5.3 \text{ \AA}$ (the distance of the first "solvation layer" in the g_{ij} 's of Fig.6), $\Delta Z_{eff} = 0.0148$ and $\epsilon_r = 4$, this relation gives $\Delta F \approx 0.040 \text{ V/\AA}$ which remarkably agrees with the estimate ΔF from Eq. (4).

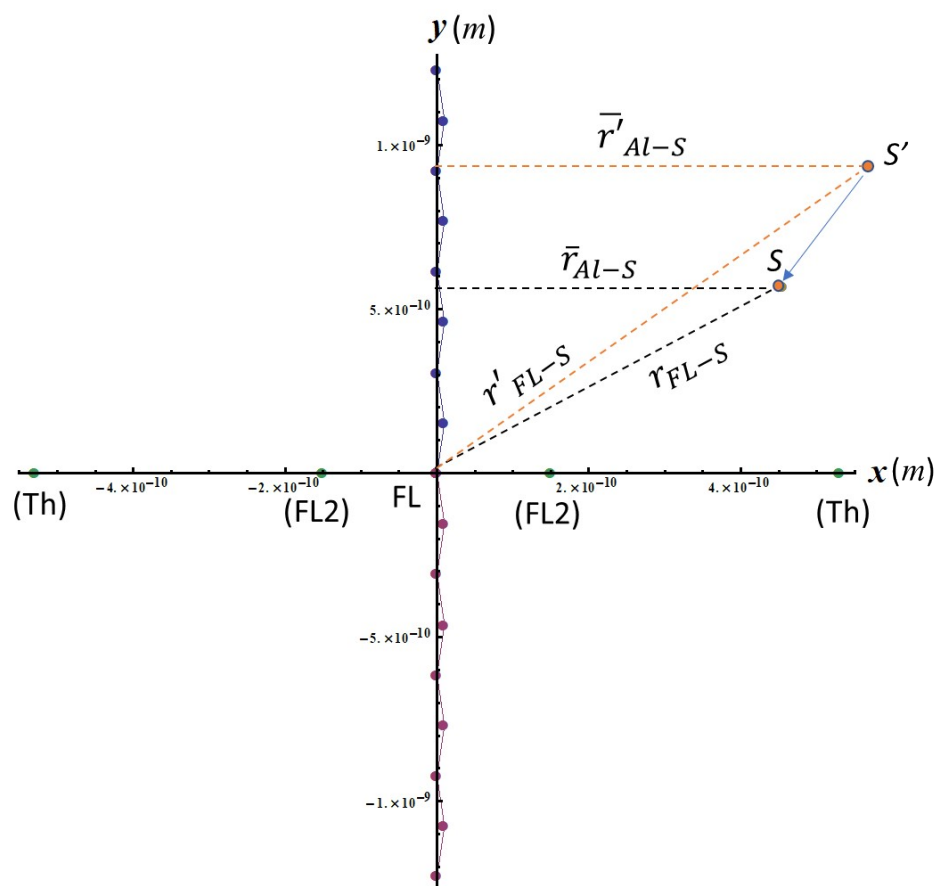


Figure S10 - Simplified two-dimensional model representing the electrostatic environment filled by the S atom (represented by the points S and S') in the vicinities of an alkyl lateral chain of the F8T2 oligomer. The coordinates r_{FL-S} (r'_{FL-S}) and \bar{r}_{FL-S} (\bar{r}'_{FL-S}) are the distances of S (S') to the center of the reference system and the average distance to the point charges in the nearest octyl side chain, respectively. The atomic charges are represented by net point charges with magnitudes given by DFT calculations. The coordinates of the alkyl charges are also in accordance with bond lengths and angles extracted from DFT. The FL point in the origin is associated to the net charge of the central pentagonal ring of the FL group whereas the FL2 represents the net charge on the remaining three carbon atoms of hexagonal ring (considering an average distance of those atoms to origin as given by DFT). Finally, the point Th represents the net charge of the closest thiophene ring belonging to the BT group. To preserve the symmetry of the system, the points FL2 and Th are also considered in the $x < 0$ interval. See Table S22 for details of charge coordinates and magnitudes.

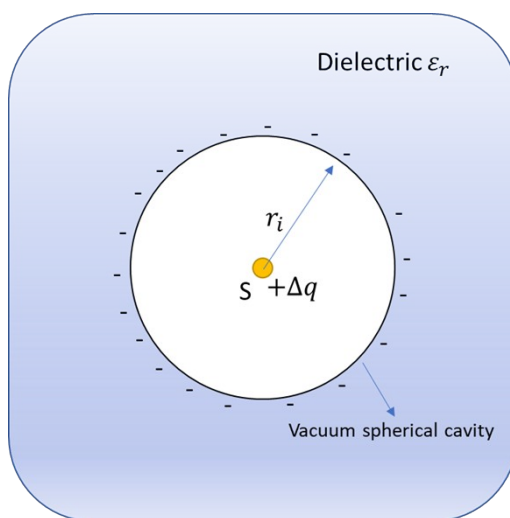


Figure S11 - Illustration of the basic model based on the Born's theory of ion-solvent interaction to estimate the electric field variation ΔF produced by a $+\Delta q$ charge increase in a central point charge representing the S atom. See text for more details.

Basic Parameters of the 2-Dimensional Model for ΔF Calculation using Point Charges

Table S5– Positions and charges of the point charges used scheme of Figure 14. The charges are taken from DFT calculations of F8T2 oligomers assuming the Millikan approximation, and wb97xd (6-31g**) level of theory.

| Point | Coordinates (Å) | | Charge(e) |
|-------|-----------------|-------------|---------------|
| | x | y | |
| Alkyl | | | |
| 1 | 0.01 | ± 1.53 | 0.026 |
| 2 | 0 | ± 3.07 | 0.008 |
| 3 | 0.01 | ± 4.61 | 0.010 |
| 4 | 0 | ± 6.15 | -0.07 |
| 5 | 0.01 | ± 7.68 | 0.009 |
| 6 | 0 | ± 9.22 | 0.012 |
| 7 | 0.01 | ± 10.75 | 0.006 |
| 8 | 0 | ± 12.29 | -0.017 |
| FL | 0 | 0 | 0.09 |
| FL2 | ± 1.5 | 0 | -0.02 |
| Th | ± 5.3 | 0 | -0.083 |

References

- [1] W. L. Jorgensen, D. S. Maxwell, and J. Tirado-Rives, "Development and testing of the OPLS all-atom force field on conformational energetics and properties of organic liquids," J. Am. Chem. Soc, vol. 118, no. 45, pp. 11225–11236, 1996.

- [2] W. L. Jorgensen, R. C. Binning Jr, and B. Bigot, "Structures and properties of organic liquids: n-butane and 1,2-dichloroethane and their conformation equilibriums," *Journal of the American Chemical Society*, vol. 103, no. 15, pp. 4393–4399, 1981.
- [3] G. A. Kaminski, R. A. Friesner, J. Tirado-Rives, and W. L. Jorgensen, "Evaluation and reparametrization of the OPLS-AA force field for proteins via comparison with accurate quantum chemical calculations on peptides," *The Journal of Physical Chemistry B*, vol. 105, no. 28, pp. 6474–6487, 2001.
- [4] H. Lorentz, "Ueber die anwendung des satzes vom virial in der kinetischen theorie der gase," *Annalen der physik*, vol. 248, no. 1, pp. 127–136, 1881.
- [5] D. Berthelot, "Sur le mélange des gaz," *Compt. Rendus*, vol. 126, pp. 1703–1706, 1898.
- [6] J.-P. Ryckaert and A. Bellemans, "Molecular dynamics of liquid n-butane near its boiling point," *Chemical Physics Letters*, vol. 30, no. 1, pp. 123–125, 1975.
- [7] J. Tirado-Rives and W. L. Jorgensen, "Performance of b3lyp density functional methods for a large set of organic molecules," *Journal of chemical theory and computation*, vol. 4, no. 2, pp. 297–306, 2008.
- [8] Z. Zheng, J.-L. Brédas, and V. Coropceanu, "Description of the charge transfer states at the pentacene/C60 interface: Combining range-separated hybrid functionals with the polarizable continuum model," *The journal of physical chemistry letters*, vol. 7, no. 13, pp. 2616–2621, 2016.
- [9] L. Benatto and M. Koehler, "Effects of fluorination on exciton binding energy and charge transport of π -conjugated donor polymers and the ITIC molecular acceptor: A theoretical study," *The Journal of Physical Chemistry C*, vol. 123, no. 11, pp. 6395–6406, 2019.
- [10] S. Cox and D. Williams, "Representation of the molecular electrostatic potential by a net atomic charge model," *Journal of Computational Chemistry*, vol. 2, no. 3, pp. 304–323, 1981.

- [11] B. H. Besler, K. M. Merz Jr, and P. A. Kollman, "Atomic charges derived from semiempirical methods," *Journal of computational chemistry*, vol. 11, no. 4, pp. 431–439, 1990.
- [12] M. P. Allen and D. J. Tildesley, *Computer Simulation of Liquids*. Oxford university press, 2017.
- [13] J.-D. Chai and M. Head-Gordon, "Long-range corrected hybrid density functionals with damped atom-atom dispersion corrections," *Physical Chemistry Chemical Physics*, vol. 10, no. 44, pp. 6615–6620, 2008.
- [14] H. E. Pence and A. Williams, "Chemspider: an online chemical information resource," 2010.
- [15] A. S. Al-Jimaz, J. A. Al-Kandary, and A.-H. M. Abdul-Latif, "Acoustical and excess properties of {chlorobenzene+ 1-hexanol, or 1-heptanol, or 1-octanol, or 1-nonanol, or 1-decanol} at (298.15, 303.15, 308.15, and 313.15) K," *Journal of Chemical & Engineering Data*, vol. 52, no. 1, pp. 206–214, 2007.
- [16] W. M. Haynes, *CRC Handbook of Chemistry and Physics*. CRC press, 2014.
- [17] W. N. Hubbard, J. W. Knowlton, and H. M. Huffman, "Combustion calorimetry of organic chlorine compounds. heats of combustion of chlorobenzene, the dichlorobenzenes and o-and p-chloroethylbenzene," *The Journal of Physical Chemistry*, vol. 58, no. 5, pp. 396–402, 1954.
- [18] P. Basařová and V. Svoboda, "Prediction of the enthalpy of vaporization by the group contribution method," *Fluid Phase Equilibria*, vol. 105, no. 1, pp. 27–47, 1995.
- [19] K. R. d. A. Sousa, L. Benatto, L. Wouk, L. S. Roman, and M. Koehler, "Effects of nonhalogenated solvent on the main properties of a solution-processed polymeric thin film for photovoltaic applications: a computational study," *Physical Chemistry Chemical Physics*, vol. 22, no. 17, pp. 9693–9702, 2020.

- [20] L. Benatto, K. R. d. A. Sousa, and M. Koehler, "Driving force for exciton dissociation in organic solar cells: The influence of donor and acceptor relative orientation," *The Journal of Physical Chemistry C*, vol. 124, no. 25, pp. 13580–13591, 2020.
- [21] L. Benatto, C. A. M. Moraes, G. Candiotto, K. R. d. A. Sousa, J. P. A. Souza, L. S. Roman, and M. Koehler, "Conditions for efficient charge generation preceded by energy transfer process in non-fullerene organic solar cells," *Journal of Materials Chemistry A*, vol. 9, no. 48, pp. 27568–27585, 2021.
- [22] R. Alessandri, J. J. Uusitalo, A. H. de Vries, R. W. Havenith, and S. J. Marrink, "Bulk heterojunction morphologies with atomistic resolution from coarse-grain solvent evaporation simulations," *Journal of the American Chemical Society*, vol. 139, no. 10, pp. 3697–3705, 2017.
- [23] O. D. Lourenço Jr., L. Benatto, C. F. N. Marchiori, H. C. Avila, N. A. Yamamoto, C. K. Oliveira, M. G. E. da Luz, M. Cremona, M. Koehler, and L. S. Roman, "Conformational change on a bithiophene-based copolymer induced by additive treatment: Application in organic photovoltaics," *The Journal of Physical Chemistry C*, vol. 121, no. 29, pp. 16035–16044, 2017.
- [24] *Quantum Physics of Atoms, Molecules, Solids, Nuclei and Particles*. R. Einsberg and R. Resnick. John Wiley & Sons, 1974.
- [25] M. N. Bellido, "On the Polarizability of the sulfur atom", *Chemical Physics Letters*, vol. 122, no. 6, pp.562-566, 1985.
- [26] *Modern Electrochemistry- An Introduction to an interdisciplinary area*. Vol. 1. John O'MBockris and Amulya K. N. Reddy. Plenum Press, New York, 1970.